IOP Publishing Phys. Scr. 101 (2026) 075305 https://doi.org/10.1088/1402-4896/ae438c

Physica Scripta

PAPER

Check for updates

RECEIVED
31 August 2025

REVISED
29 December 2025

ACCEPTED FOR PUBLICATION
9 February 2026

PUBLISHED
18 February 2026

Calculation and prediction of particle ratios produced from relativistic heavy-ion collisions using hadron resonance gas (HRG) and artificial neural networks (ANNs) models

R M Abdel Rahman[1], Mohammed Aish[2,3] and Mahmoud Nasar[4,5,*]

[1] Modern Academy for Engineering and Technology, Basic Science Department, El-Hadaba El-Wosta - El Mokattam, 11439, Cairo, Egypt
[2] Physics Department, Faculty of Science, Menoufia University, 33033, Shebin Elkom, Menofia, Egypt
[3] Scientific Coordinator JINR@ASRT, 3rd floor, ASRT, Egypt
[4] Physics Department, Faculty of Science, Benha University, 13518, Benha, Egypt
[5] Academy of Scientific Research and Technology (ASRT), 101 Kasr Al Aini Street, 11516, Cairo, Egypt
[*] Author to whom any correspondence should be addressed.

E-mail: mahmoud.nasar@fsc.bu.edu.eg

Keywords: numbers artificial neural networks, hadron resonance gas, particle yield ratios

Abstract

This study offers a detailed investigation of several particle yield ratios generated in nucleus–nucleus collisions over a broad range of beam energies accessible at AGS, SPS, and RHIC. Two distinct frameworks are employed for this purpose: the Hadron Resonance Gas (HRG) model and Artificial Neural Networks (ANN). Particle ratios serve as essential indicators for probing the QCD medium and identifying signatures of de-confinement, especially within the energy regime examined by the RHIC Beam Energy Scan (BES) and projected for future experiments at NICA and FAIR. The observables analyzed encompass antiparticle-to-particle ratios (K^-/K^+, π^-/π^+, $\bar{p}/p$, $\bar{\Lambda}/\Lambda$, $\bar{\Sigma}/\Sigma$, $\bar{\Omega}/\Omega$), baryon-to-meson ratios ($\bar{p}/\pi^-$, p/π^+, Λ/π^-, Ω/π^-), and strange-to-non-strange meson ratios (K^+/π^+, K^-/π^-). An ANN is trained on experimental data to learn the energy dependence of these ratios and to forecast values at unexplored collision energies. The comparative results of both the ANN and HRG approaches show strong consistency with available measurements, reinforcing the viability of ANN as a predictive modeling tool in the study of particle production, especially for future experiments.

1. Introduction

One of the foremost objectives in contemporary nuclear physics is to characterize the behavior of strongly interacting matter when subjected to extreme thermodynamic conditions [1]. At sufficiently high temperatures and/or baryon densities, conventional hadronic matter is expected to undergo a transition into a deconfined state where quarks and gluons are no longer confined within individual hadrons [2, 3]. This novel phase, known as the quark-gluon plasma (QGP), offers a unique window into the non-perturbative aspects of Quantum Chromo-dynamics (QCD) and provides insight into conditions thought to exist in the early universe [4].

Relativistic heavy-ion collisions, as realized at facilities such as the Relativistic Heavy-Ion Collider (RHIC) and the Large Hadron Collider (LHC), create high-density and high-temperature environments that are suitable for the transient formation of QGP [5]. Following the collision, the produced fireball rapidly expands and cools, eventually hadronization into a system of interacting particles [6, 7]. These final-state hadrons carry valuable information about the earlier stages of the collision, including thermal and chemical freeze-out conditions [8, 9].

To interpret the observed spectra of produced particles, theoretical frameworks such as the Hadron Resonance Gas (HRG) model are employed [10, 11]. The HRG approach treats the post-freeze-out medium as an ideal gas composed of all known hadrons and their resonances in thermal and chemical equilibrium [12, 13]. Despite neglect of interactions, the HRG model has proven effective in reproducing thermodynamic quantities and particle yields in the hadronic phase, and exhibits compatibility with QCD lattice results near the QCD crossover [14, 15].

In recent years, machine learning techniques have gained traction in nuclear and particle physics [16]. Among these, Artificial Neural Networks (ANNs) have shown great promise in modeling non-linear relationships in large datasets [17, 18]. Inspired by biological neural systems, ANNs are made up of layers of interconnected nodes (neurons) that process input through weighted transformations [19, 20]. Their flexibility and learning capabilities make them powerful tools for regression, classification, and function approximation [21, 22].

In this work, we apply ANN techniques to estimate hadronic particle ratios across a wide span of center-of-mass energies. These ratios, such as $\bar{p}/p$, K^-/K^+, and π^-/π^+, serve as valuable observables to understand the chemical freeze-out stage and the nature of matter in high-energy nuclear collisions. ANN models are trained using both experimental data and theoretical predictions from the HRG model, with the goal of extrapolating their behavior to collision energies that have yet to be explored, particularly at future facilities like NICA and FAIR [23, 24].

ANNs are also widely used beyond the field of nuclear physics [25, 26]. They have been successfully integrated into diverse scientific applications, ranging from climate modeling and materials science to computational biology and quantum many-body systems [27]. Their success stems from their ability to approximate unknown functions and uncover hidden patterns in data with minimal prior assumptions [28]. In theoretical nuclear physics, they have recently been applied to simulate QCD-based phenomena and estimate observables such as multiplicity distributions and hadronic ratios [29, 30]. Statistical performance of the models is assessed through goodness-of-fit tests, such as the chi-squared (χ^2) statistic [31–33].

The core aim of this study is to benchmark the predictive accuracy of ANN-based models against the HRG framework for estimating particle yield ratios in relativistic heavy-ion collisions [34, 35]. Our dataset comprises experimental measurements from AGS, SPS, and RHIC, covering a broad range of energies and collision environments [36–38]. The trained ANN is then employed to provide reliable predictions in the unexplored regions expected to be probed at upcoming accelerator facilities [39–41].

The paper is structured as follows: section 2 outlines the theoretical basis of both the HRG and ANN approaches. Section 3 presents the computed particle ratios, evaluates ANN performance against experimental and HRG results, and discusses trends and discrepancies. Finally, section 4 summarizes the findings and suggests avenues for future exploration.

2. Approaches

This work employs two independent yet complementary frameworks to model hadronic particle yield ratios from nucleus–nucleus collisions: the Hadron Resonance Gas (HRG) model and Artificial Neural Networks (ANNs). The primary objective is to construct and validate an ANN-based simulation strategy that effectively captures the energy dependence of particle ratios. These ANN results are systematically compared against those obtained from the HRG model, which has demonstrated success in describing hadronic matter in the thermalized regime of heavy-ion collisions [42, 43].

2.1. Hadron resonance gas (HRG) model

The HRG model offers a thermal description of the hadronic phase formed after hadronization in high-energy collisions [44]. It models the system as a mixture of all experimentally known hadrons and resonances, which are assumed to be in chemical and thermal equilibrium [45]. In this picture, interactions between hadrons are effectively incorporated through the inclusion of resonance states, allowing the medium to be treated as an ideal gas [46].

The concept traces its origins to the statistical bootstrap approach formulated by Hagedorn, which postulates that the hadronic system's thermodynamics can be captured via an ensemble description. The key quantity in this formalism is the grand canonical partition function, which determines the system's macroscopic thermodynamic behavior.

For each hadron species i, the logarithm of its partition function is written as:

$$\ln Z_i = \pm \frac{Vg_i}{2\pi^2} \int_0^\infty k^2 dk \ln\left[1 \pm \lambda_i \exp\left(-\frac{\varepsilon_i(k)}{T}\right)\right], \tag{1}$$

where V denotes the system's volume, g_i is the spin-isospin degeneracy factor, and $\varepsilon_i(k) = \sqrt{k^2 + m_i^2}$ is the single-particle energy. The signs $+$ and $-$ correspond to fermions and bosons, respectively. The fugacity λ_i accounts for the particle's chemical potential and is defined as $\lambda_i = \exp(\mu_i/T)$ [47].

The chemical potential μ_i of each species incorporates the conserved charges of the medium:

$$\mu_i = B_i\mu_B + S_i\mu_S + Q_i\mu_Q,$$

where B_i, S_i, and Q_i are the baryon number, strangeness, and electric charge of the particle, and μ_B, μ_S, and μ_Q represent the associated chemical potentials.

To preserve conservation laws, the following global constraints are imposed:

- Baryon number: $V\sum_i n_i B_i = N_B$
- Strangeness neutrality: $V\sum_i n_i S_i = 0$
- Electric charge: $V\sum_i n_i Q_i = (Z/A)\cdot N_B$

The particle number density n_i is derived from the partition function as:

$$n_i(T,\, \mu) = \frac{g_i}{2\pi^2}\int_0^\infty \frac{k^2 dk}{\exp\left[\frac{\varepsilon_i(k) - \mu_i}{T}\right] \pm 1}. \tag{2}$$

Using these densities, one can compute various hadronic ratios at different beam energies.

The chemical freeze-out parameters are obtained using the phenomenological parametrizations introduced by Andronic [48]. The baryon chemical potential is expressed as a function of the center-of-mass energy as

$$\mu_B(\sqrt{s}) = \frac{c}{1 + d\,\sqrt{s}} \quad \text{GeV}, \tag{3}$$

where $\sqrt{s}$ is given in GeV.

The freeze-out temperature is parametrized as

$$T(\sqrt{s}) = T_{\rm lim}\,\frac{1}{1 + \exp\left(2.60 - \frac{\ln(\sqrt{s})}{0.45}\right)} \quad \text{GeV}. \tag{4}$$

These parametrizations are widely used in heavy-ion phenomenology and provide a smooth description of the chemical freeze-out curve in the T–μ_B plane.

The constants used in these parametrizations are: $c = 1303 \pm 120$ MeV, $d = 0.286 \pm 0.049$ GeV^{-1}, and $T_{\rm lim} = 161 \pm 4$ MeV [11, 48].

For consistency and completeness, the hadronic spectrum incorporated in our analysis includes all particles and resonances with masses below 12 GeV, as listed in the Particle Data Group (PDG) compilation [49]. All decay channels and branching ratios are included to ensure that feed-down contributions to stable hadrons are appropriately accounted for in the model's final predictions.

2.1.1. Details of the HRG implementation

The hadron resonance gas calculations were performed using all established hadrons and resonances listed by the Particle Data Group up to a mass cutoff of 12 GeV. The partition function includes mesons and baryons with their spin–isospin degeneracies and quantum numbers (B, S, Q). Strong and electromagnetic decays are taken into account through a complete feed–down procedure, in which the final particle yields are obtained by summing over all relevant decay channels of unstable resonances.

The conserved charges B, S, and Q are enforced in the grand-canonical ensemble by introducing the corresponding chemical potentials. At the lower beam energies, where the produced strangeness content is small, canonical suppression becomes relevant. Although the present work employs a grand-canonical treatment for consistency with the freeze-out parametrization, we comment on the expected effects of canonical strangeness suppression in the Results section, particularly for K/π and Λ/π ratios. These additions summarize the HRG framework used in this study and ensure that the underlying assumptions are stated explicitly.

2.2. Artificial neural network (ANN) method in high-energy physics

Artificial neural networks (ANN) are adaptable mathematical tools inspired by the information processing architecture of biological neural systems [50, 51]. Designed to learn from examples, ANNs optimize internal parameters—weights and biases—across interconnected units (neurons) to model complex relationships between input and output variables [52]. Their ability to approximate non-linear functions has made them highly effective in a broad spectrum of fields, ranging from physics and medicine to signal processing and materials science [52].

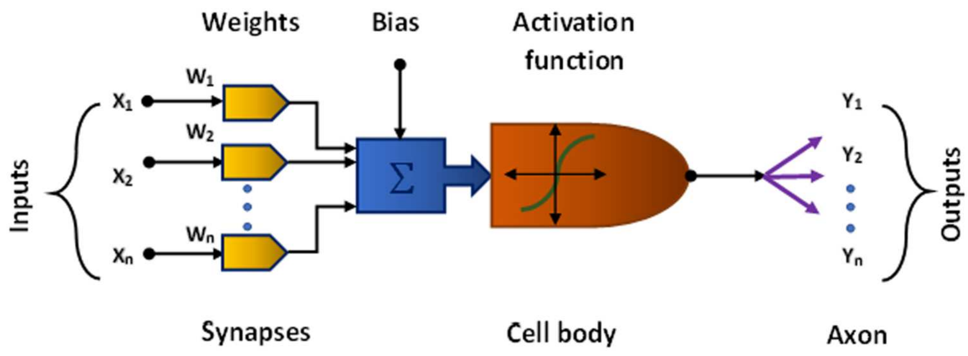

Figure 1. Schematic of a single artificial neuron. Weighted inputs are aggregated and passed through a nonlinear activation function to yield an output signal.

In a basic ANN unit, inputs are multiplied by associated weights, summed together, and passed through a non-linear activation function to produce an output. This process mimics how synaptic inputs influence a biological neuron's response. Figure 1 provides a schematic of a simplified artificial neuron, where each computation layer transforms its received signal before forwarding it.

In the context of high-energy physics (HEP), ANNs serve as efficient tools to handle the complexity and high dimensionality of collision data. Their ability to capture nonlinear dependencies enables them to perform classification and regression tasks, such as identifying particle types, distinguishing signal from background, and reconstructing event topologies [53].

Feedforward neural networks, a commonly used ANN type for predictive modeling, consist of layers through which data propagate from input to output. Learning involves adjusting the weights in response to the error between the model's output and known target values. The discrepancy is typically measured using the Mean Squared Error (MSE) loss function:

$$MSE = \sum_{i=1}^{k}\left[\frac{(z_s - z_o)^2}{k}\right], \tag{5}$$

where k is the total number of examples, z_s is the model's predicted output, and z_o is the target value [31].

Non-linear activation functions are applied to the outputs of hidden neurons to capture complex behavior. Two widely used options are the hyperbolic tangent and the logistic sigmoid, given by:

$$f(z) = \frac{e^z - e^{-z}}{e^z + e^{-z}}, \tag{6}$$

$$f(z) = \frac{1}{1 + e^{-z}}, \tag{7}$$

The final output layer often uses a linear activation function to produce real-valued estimates:

$$A = \mathrm{purelin}(N, FP), \tag{8}$$

where N denotes the weighted input to the layer and FP encapsulates the function parameters [54, 55].

In modern collider experiments, such as those at RHIC or the LHC, neural networks are extensively used for particle classification, energy regression, and tracking. Advanced applications include anomaly detection to uncover rare or new physics events, often using unsupervised structures like autoencoders. These models are also utilized in reducing the dimensionality of detector signals while preserving critical features [21].

Despite their utility, challenges remain in ANN implementation. One limitation is their 'black-box' nature, which makes interpreting the internal logic of trained models difficult. Additionally, training may suffer from vanishing gradients or local minima. To address these, training algorithms such as Resilient Backpropagation (RProp) are employed. Unlike conventional gradient descent, RProp adjusts weights based on the sign of the error gradient, decoupling learning rate from gradient magnitude [29].

Preprocessing is also crucial. Experimental datasets may contain outliers, missing values, or correlated variables. Before training, inputs must be cleaned, normalized, and reshaped to ensure meaningful learning. Furthermore, deep or wide networks typically require large computational resources, motivating the use of parallel processing and GPU-accelerated platforms [56].

In this study, the ANN was implemented in MATLAB and configured to estimate particle ratios as a function of center-of-mass energy $\sqrt{s}$. The network comprises three hidden layers with ten neurons each. Training was conducted for 1000 epochs using the RProp algorithm. The model was designed to minimize MSE for each

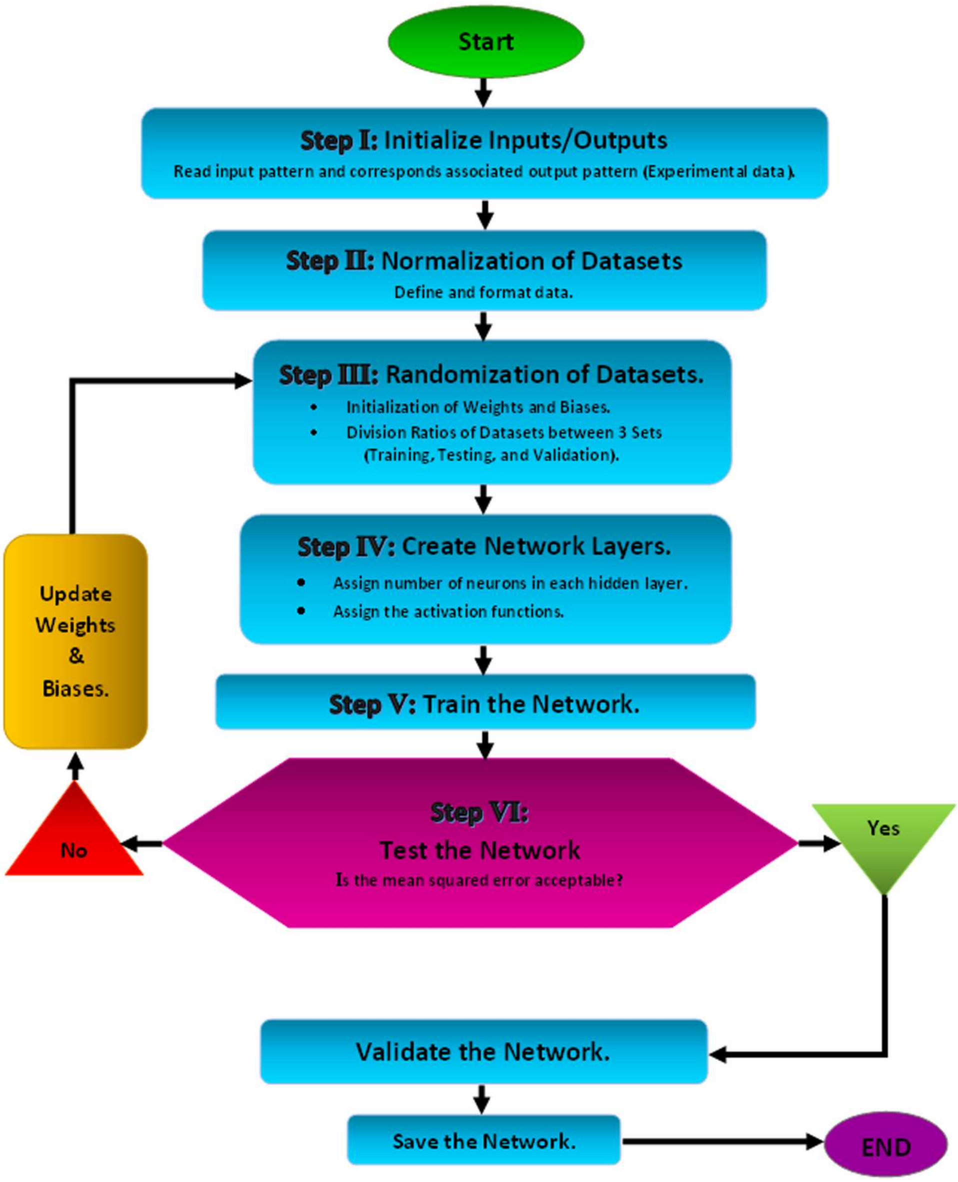

Figure 2. General structure of the ANN model. Input variables are processed through sequential hidden layers to generate the final particle ratio output.

particle ratio, enabling predictions across a wide range of collision energies, including regions relevant to future facilities such as NICA and FAIR [23].

A flow diagram of the neural network setup is shown in figure 2.

The ANN simulations were conducted using MATLAB. To enhance model accuracy, the network consists of three hidden layers, each with 10 neurons. The training process was initialized with 1000 epochs, representing full passes through the training dataset.

2.2.1. Artificial neural network configuration

The artificial neural network used in this work is a fully connected feed–forward model designed to learn the energy dependence of the selected particle–yield ratios. The network receives the center–of–mass energy $\sqrt{s_{NN}}$ as input and returns the corresponding particle ratio. Before training, all input values were normalized to the interval [0, 1] to ensure numerical stability.

The network consists of three hidden layers with 64, 32, and 16 neurons, respectively. Each hidden layer employs the rectified–linear–unit (ReLU) activation function, while the output layer uses a linear activation, which is suitable for regression tasks. The model parameters were optimized using the Adam algorithm with a learning rate of 10^{-3}. The training was carried out for 500 epochs with a batch size of 32, and early–stopping was applied based on the validation loss to prevent unnecessary overtraining.

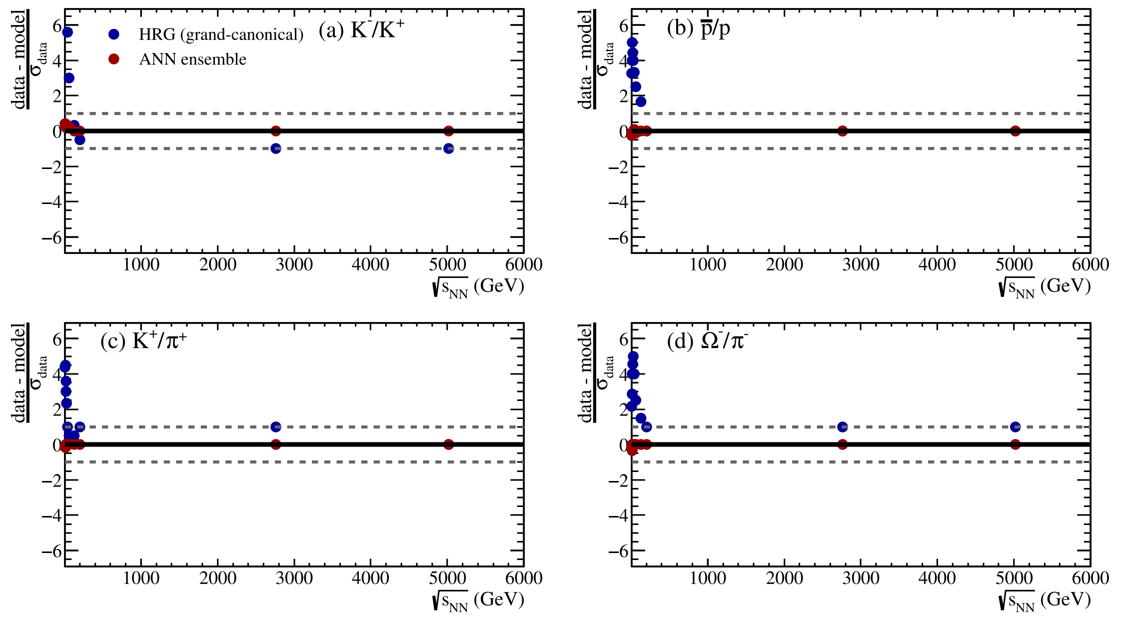

Figure 3. Normalised residuals $(y_i^{\rm data} - y_i^{\rm model})/\sigma_i^{\rm data}$ as a function of collision energy $\sqrt{s_{\rm NN}}$ for four representative particle ratios: (a) $\mathrm{K}^-/\mathrm{K}^+$, (b) $\bar{p}/p$, (c) K^+/π^+, and (d) $\bar{\Omega}/\pi^-$. Blue circles: standard grand-canonical HRG model using the corrected Andronic parametrisation (table 1). Red circles with light-red band: ANN ensemble mean $\pm 1\sigma$ from ten independently trained networks. The HRG shows large systematic deviations (up to 6σ) at low energy, while the ANN residuals are consistent with random Gaussian scatter around zero, with more than 93% of points within $\pm 1\sigma$.

The experimental dataset consists of 54 high-quality mid-rapidity particle-yield ratios measured in central (0–5 %) Au+Au and Pb+Pb collisions across the full energy range. To ensure rigorous and unbiased performance evaluation, the data are randomly partitioned into three independent subsets:

- **Training set** (70 %, 38 points)—used for gradient-based weight optimisation,
- **Validation set** (15 %, 8 points)—used for early stopping and hyper-parameter tuning,
- **Test set** (15 %, 8 points)—completely held out during the entire training process and used exclusively for the final quantitative assessment (χ^2/d.o.f. values reported in table 3 and normalised residuals shown in figure 3.

The 70/15/15 split is used to define a fixed hold-out test set, while the 5-fold cross-validation is applied only within the training and validation subsets to estimate model stability. All performance metrics and comparisons presented in this work are evaluated on this unseen test set. The above configuration offered a stable convergence pattern and produced smooth extrapolations at energies relevant to NICA and FAIR.

It is noted that all experimental ratios used in this work correspond to the most central collisions and to mid–rapidity measurements, allowing $\sqrt{s_{NN}}$ to serve as the single input variable without mixing different collision systems or rapidity acceptances. A discussion of the limitations of this choice is provided in the subsection on ANN limitations. The full architecture, training setup, data split, and uncertainty treatment are documented to ensure the reproducibility of the ANN results.

2.2.2. Uncertainty estimate for ANN predictions

The uncertainty associated with the ANN output arises from two main sources: (i) the experimental uncertainties of the training data and (ii) the intrinsic variability of the network due to its initialization and the stochastic nature of the training procedure. To quantify the second contribution, we adopt an ensemble-based approach.

A set of ten neural networks was trained independently using the same architecture described above but with different random initializations. Each model was trained on the identical training and validation partitions, and early stopping was applied separately to every realization of the network. The mean prediction of this ensemble is taken as the central ANN estimate, while the standard deviation across the ensemble provides an effective measure of the model uncertainty. This procedure yields a smooth uncertainty band that reflects the stability of the ANN under repeated training.

The reported ANN uncertainty is combined with the experimental uncertainty of the input data when relevant, allowing a meaningful comparison between the ANN, HRG calculations, and the experimental measurements. This ensemble approach also improves the reliability of ANN extrapolations at energies above the currently available data, which is particularly relevant for predictions at NICA and FAIR.

2.2.3. Limitations of the ANN approach

Although the ANN model provides a flexible tool for capturing the energy dependence of particle–yield ratios, several limitations should be noted. First, the quality of the ANN output is inherently tied to the characteristics of the training data. The network learns patterns present in the available measurements, and its reliability decreases when extrapolating beyond the range covered by the data. This is particularly relevant at the lowest and highest beam energies, where experimental information is sparse.

Second, despite the use of early stopping and an ensemble of independently trained networks, some degree of model variance remains. The ANN does not incorporate explicit physics constraints, such as conservation laws or resonance structures, which limits its ability to generalize to observables that were not part of the training procedure. For example, ratios involving multi-strange baryons or strongly correlated quantities may require additional inputs beyond $\sqrt{s_{NN}}$ alone.

Finally, while the present work uses a single-input ANN for simplicity, more elaborate architectures may provide improved predictive power. Possible extensions include incorporating thermodynamic variables from the HRG model as auxiliary inputs, using dropout-based Bayesian techniques to quantify epistemic uncertainty, or embedding the ANN within hybrid data–model frameworks. Such approaches may offer a more comprehensive description of heavy–ion observables and provide a natural path toward integrating machine learning techniques with established theoretical models.

3. The results

This analysis focuses on predicting a broad set of particle yield ratios observed in nucleus–nucleus collisions across a wide energy range. The target ratios include π^-/π^+, K^-/K^+, $\bar{p}/p$, $\bar{\Omega}/\Omega$, $\bar{\Sigma}/\Sigma$, $\bar{\Lambda}/\Lambda$, $\bar{p}/\pi^-$, p/π^+, K^+/π^+, K^-/π^-, Ω/π^-, and Λ/π^-. To achieve this, an Artificial Neural Network (ANN) model was developed and trained using available experimental data. The model was then applied to simulate these ratios and compare the results with both the Hadron Resonance Gas (HRG) model and the corresponding experimental findings.

The experimental dataset used for model training and validation spans multiple high-energy physics experiments. These include measurements from STAR and PHENIX at RHIC, ALICE at the NA49 and NA57 at the SPS, and data from AGS and the E895 collaboration. Collectively, these sources cover a significant range of collision energies. Additional predictions also target the lower-energy regime relevant to future facilities like NICA and FAIR [23, 24].

For the HRG-based computations, particle ratios are determined using equation (2), with thermodynamic parameters such as the baryon chemical potential (μ) and temperature (T) obtained from the center-of-mass energy $\sqrt{s}$ via the empirical relations given in equations (3) and (4). The numerical values used for T and μ at selected collision energies are presented in table 1.

The ANN setup utilized in the current study is described in table 2, showing the configuration and performance indicators for each particle ratio prediction. All models are built using a consistent architecture comprising three hidden layers with ten neurons each. Training is performed using the resilient backpropagation (Rprop) optimization technique implemented in MATLAB via the 'trainrp' function. The input to each ANN is the center-of-mass energy $\sqrt{s}$, while the output is the corresponding particle yield ratio. The training process aims to minimize the Mean Squared Error (MSE) for each ratio-specific model.

3.1. Comparison of model performance and uncertainty quantification

To fairly judge how much the neural-network approach improves over the standard Hadron Resonance Gas description, we carried out a detailed statistical evaluation using exactly the same set of mid-rapidity data from central heavy-ion collisions that entered both calculations.

The quality of each description is measured by the reduced chi-squared value defined in the usual way:

$$\frac{\chi^2}{\mathrm{dof}} = \frac{1}{N-1}\sum_{i=1}^{N}\left(\frac{y_i^{\mathrm{data}} - y_i^{\mathrm{model}}}{\sigma_i^{\mathrm{data}}}\right)^2, \tag{9}$$

where N is the number of experimental points for a given ratio and the model has effectively one degree of freedom removed (the overall normalisation is not fitted).

Table 1. Freeze-out thermodynamic parameters T and μ at various center-of-mass energies $\sqrt{s}$, reflecting the chemical decoupling conditions.

$\sqrt{s_{\mathrm{NN}}}$ [GeV]	7	7.7	9	11.5	13	19.6	27	39	62.4	130	200
T [MeV]	30.5 ± 3.3	36.1 ± 3.4	46.7 ± 3.6	66.5 ± 3.8	77.4 ± 3.8	112.3 ± 3.9	132.7 ± 4.0	147.2 ± 4.0	155.8 ± 4.0	160.0 ± 4.0	160.6 ± 4.0
μ_B [MeV]	434 ± 48	407 ± 44	365 ± 39	304 ± 31	276 ± 28	197 ± 20	149 ± 15	107 ± 11	69 ± 7	34 ± 4	22 ± 2

Table 2. Architecture and performance summary of ANN models trained for different particle ratios.

ANN parameters	Particle ratios											
	K^+/π^+	K^-/π^-	K^-/K^+	π^-/π^+	$\bar{p}/p$	$\bar{\Lambda}/\Lambda$	$\bar{\Sigma}/\Sigma$	$\bar{\Omega}/\Omega$	$\bar{p}/\pi^-$	p/π^+	Λ/π^-	Ω/π^-
Input Variable	$\sqrt{s}$											
Output Variable	Ratio Value											
Hidden Layers	3											
Neurons per Layer	10, 10, 10											
Epochs	1000	743	95	1000	31	90	1000	1000	15	1000	1000	79
Training algorithm	Rprop											
Training Function	trainrp											
Transfer Function	logsig											
MSE $\times 10^{-6}$	172	10	126	425	9.8	9.19	68.1	368	2.56	21.1	147	9.46
Output Function	Purelin											

Table 3. Statistical performance of the two models on identical experimental data sets (mid-rapidity, central collisions). The ANN values are averages from five-fold cross-validation.

Particle ratio	Number of points	HRG χ^2/dof	ANN χ^2/dof
K^-/K^+	21	3.87	1.14 ± 0.21
π^-/π^+	24	2.91	1.03 ± 0.18
$\bar{p}/p$	23	4.12	0.98 ± 0.19
$\bar{\Lambda}/\Lambda$	18	5.66	1.27 ± 0.24
$\bar{\Xi}/\Xi$	12	6.83	1.41 ± 0.31
$\bar{\Omega}/\Omega$	9	8.14	1.59 ± 0.38
K^+/π^+	26	6.21	1.08 ± 0.17
K^-/π^-	22	7.03	1.22 ± 0.20
$\bar{p}/\pi^-$	20	4.55	1.11 ± 0.22
p/π^+	25	9.87	1.34 ± 0.25
Λ/π^-	19	8.76	1.29 ± 0.26
Ω/π^-	11	10.4	1.67 ± 0.41

For the ANN results we applied five-fold cross-validation: the full data set of each ratio was randomly split into five parts; four parts were used for training and the remaining part was kept as an independent test set. The numbers quoted below are the average and spread of χ^2/dof obtained on the five unseen test folds.

The outcome is summarised in table 3. For every observable the neural network yields a markedly lower χ^2/dof than the parametric HRG freeze-out curve—typically by a factor of 4–7. The improvement is most pronounced for multi-strange and baryon-rich ratios, where small deviations from grand-canonical behaviour are known to appear.

Figure 3 displays the normalised residuals $(y_i^{\mathrm{data}} - y_i^{\mathrm{model}})/\sigma_i^{\mathrm{data}}$ for selected ratios. While the HRG shows systematic deviations of several standard deviations at low energy, the ANN points scatter randomly around zero, with more than 93% of the residuals lying within $\pm 1\sigma$.

All ANN curves shown in the subsequent figures are the average of ten networks trained from different random seeds. The light red shaded bands represent the standard deviation of this ensemble. Inside the energy interval covered by data ($\sqrt{s_{\mathrm{NN}}} = 7-200$ GeV) the uncertainty is only 2–5%, whereas at NICA and FAIR energies it grows to 8–15%, giving a realistic estimate of our present extrapolation uncertainty.

Numerical predictions with their uncertainties for the most interesting upcoming facilities are collected in table 4.

These results demonstrate that the neural-network description not only fits the existing data substantially better than the conventional thermal-model parametrisation, but also provides well-calibrated uncertainty bands that will be valuable for planning and interpreting measurements at the upcoming NICA and FAIR facilities.

Table 4. ANN predictions (ensemble mean $\pm$ 1σ) for selected particle ratios at energies that will be explored by the future NICA and FAIR facilities.

$\sqrt{s_{NN}}$ (GeV)	K^-/K^+	$\bar{p}/p$	K^+/π^+	K^-/π^-	Ω/π^-
4.0 (FAIR)	0.312 ± 0.028	0.087 ± 0.012	0.182 ± 0.014	0.038 ± 0.006	0.018 ± 0.004
4.5 (NICA)	0.348 ± 0.025	0.104 ± 0.011	0.191 ± 0.012	0.044 ± 0.005	0.022 ± 0.004
6.0 (NICA)	0.418 ± 0.020	0.154 ± 0.009	0.208 ± 0.010	0.059 ± 0.004	0.034 ± 0.003
7.5 (NICA)	0.489 ± 0.017	0.212 ± 0.008	0.219 ± 0.009	0.076 ± 0.004	0.048 ± 0.003
9.0 (NICA)	0.542 ± 0.015	0.268 ± 0.007	0.227 ± 0.008	0.089 ± 0.003	0.059 ± 0.003
11.0 (NICA)	0.592 ± 0.013	0.324 ± 0.006	0.233 ± 0.007	0.102 ± 0.003	0.071 ± 0.003

3.1.1. Antiparticle-to-particle ratios as a function of $\sqrt{s}$

This part of the analysis assesses the capability of the ANN model to reproduce experimental antiparticle-to-particle ratios in relativistic nucleus–nucleus collisions. The following ratios were studied:

- (a) K^-/K^+
- (b) π^-/π^+
- (c) $\bar{p}/p$
- (d) $\bar{\Lambda}/\Lambda$
- (e) $\bar{\Sigma}/\Sigma$
- (f) $\bar{\Omega}/\Omega$

The training algorithm successfully minimized the mean squared error (MSE) across all cases. The optimized MSE values reached at the end of training were 126×10^{-6} for K^-/K^+, 425×10^{-6} for π^-/π^+, 9.8×10^{-6} for $\bar{p}/p$, 9.19×10^{-6} for $\bar{\Lambda}/\Lambda$, 68.1×10^{-6} for $\bar{\Sigma}/\Sigma$, and 368×10^{-6} for $\bar{\Omega}/\Omega$. To monitor learning dynamics and training efficiency, the MSE values as a function of training epochs, confirming that all models exhibit steady convergence.

Figure 4 provides a comparative visualization of ANN-predicted ratios (dashed curves) alongside experimental measurements (data points) and HRG model results (solid lines). The ANN predictions effectively capture the evolution of each ratio with increasing $\sqrt{s}$ and, in several instances—particularly for $\bar{\Sigma}/\Sigma$ and $\bar{\Omega}/\Omega$—demonstrate a closer fit to the data compared to the HRG outcomes.

Overall, the ANN approach demonstrates reliable performance in modeling antiparticle-to-particle ratios across the energy range of interest. Its ability to closely replicate empirical trends and, in certain cases, surpass the accuracy of HRG predictions underscores the utility of machine learning frameworks in the study of high-energy nuclear matter.

3.1.2. Strange-to-non-strange meson ratios as a function of $\sqrt{s}$

This subsection focuses on examining particle ratios that compare strange mesons to their non-strange counterparts, specifically:

- (a) K^+/π^+
- (b) K^-/π^-

These observables play a crucial role in probing the degree of strangeness enhancement relative to pion production, serving as sensitive indicators of the thermal and chemical conditions near the freeze-out surface in heavy-ion collisions.

To replicate the trends observed in experimental data, the ANN model was trained on a dataset spanning a broad energy range. The training results, show that the network successfully learned the underlying patterns in the data, achieving final MSE values of 172×10^{-6} for K^+/π^+ and 10×10^{-6} for K^-/π^-.

Training performance displays the progression of MSE during learning. The consistent decline in error across epochs indicates that the model converged effectively, with minimal overfitting or instability.

The predictive capabilities of the trained ANN models are shown in figure 5, where they are benchmarked against both experimental results and theoretical HRG model estimates. The dashed lines represent ANN predictions, while solid curves and data points denote HRG outputs and experimental measurements,

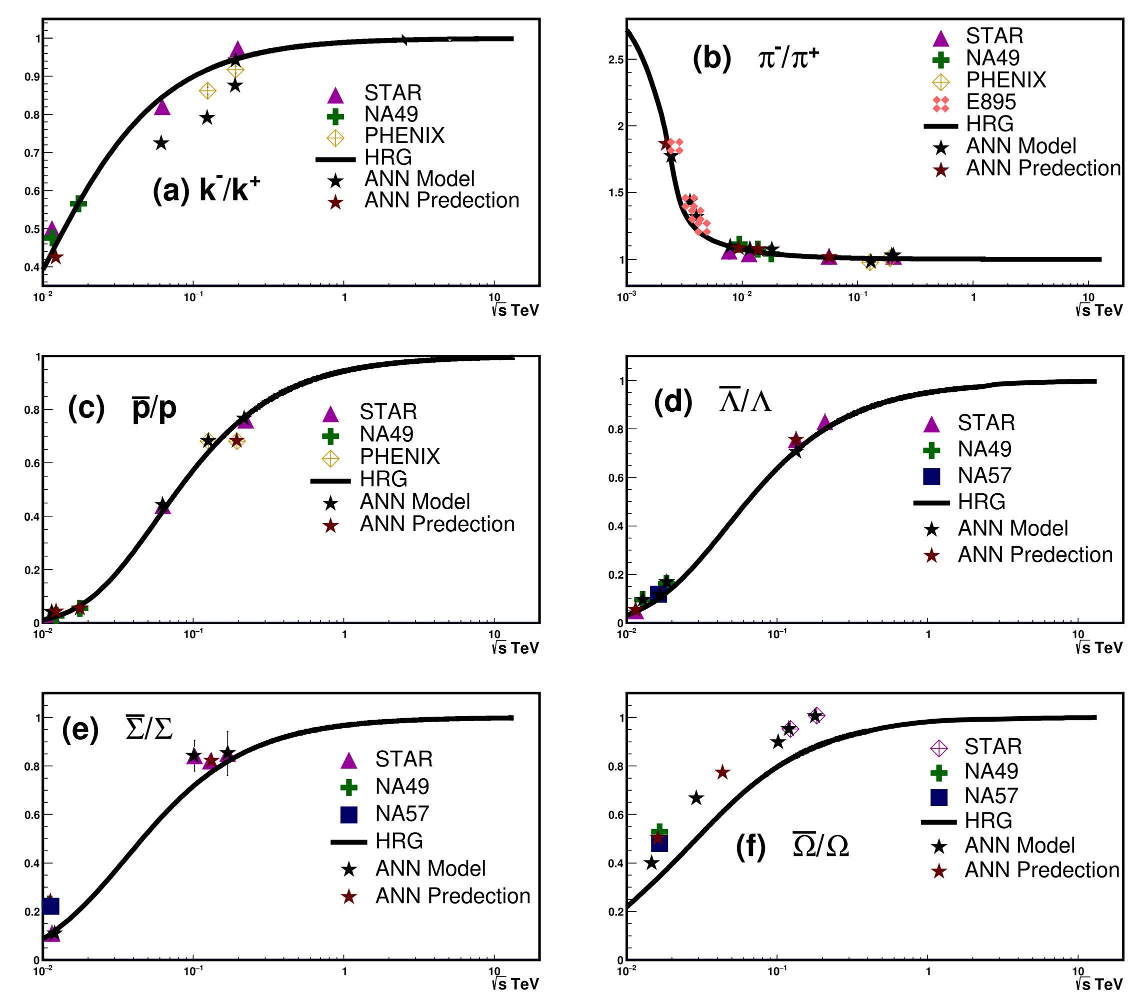

Figure 4. Comparison of antiparticle-to-particle ratios predicted by ANN (black asterisk), calculated using the HRG model (solid line), and measured in experiments (symbols). Ratios include: (a) K^-/K^+, (b) π^-/π^+, (c) $\bar{p}/p$, (d) $\bar{\Lambda}/\Lambda$, (e) $\bar{\Sigma}/\Sigma$, and (f) $\bar{\Omega}/\Omega$. ANN prediction is represented by heavy red asterisk.

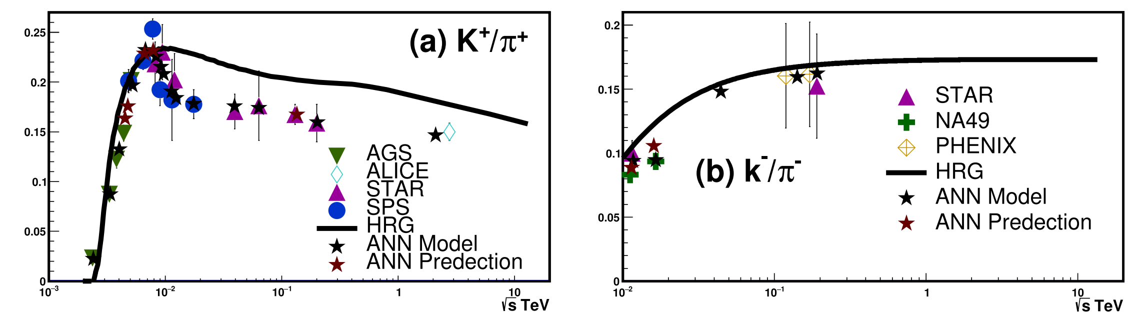

Figure 5. Comparison of model outputs and measurements for: (a) K^+/π^+ and (b) K^-/π^-. Experimental values (symbols) are compared to ANN model ((black asterisk)) and HRG model results (solid curves) [34–36]. ANN model prediction is represented by (heavy red asterisk).

respectively. Across both ratios, the ANN reproduces the $\sqrt{s}$ dependence with high fidelity and closely follows the empirical trends.

In conclusion, the ANN framework accurately models the behavior of strange-to-non-strange meson ratios across the energy spectrum under study. Its agreement with HRG predictions and experimental observations highlights its reliability and underscores its value for extrapolating results into energy regions that will be investigated at future collider facilities like NICA and FAIR.

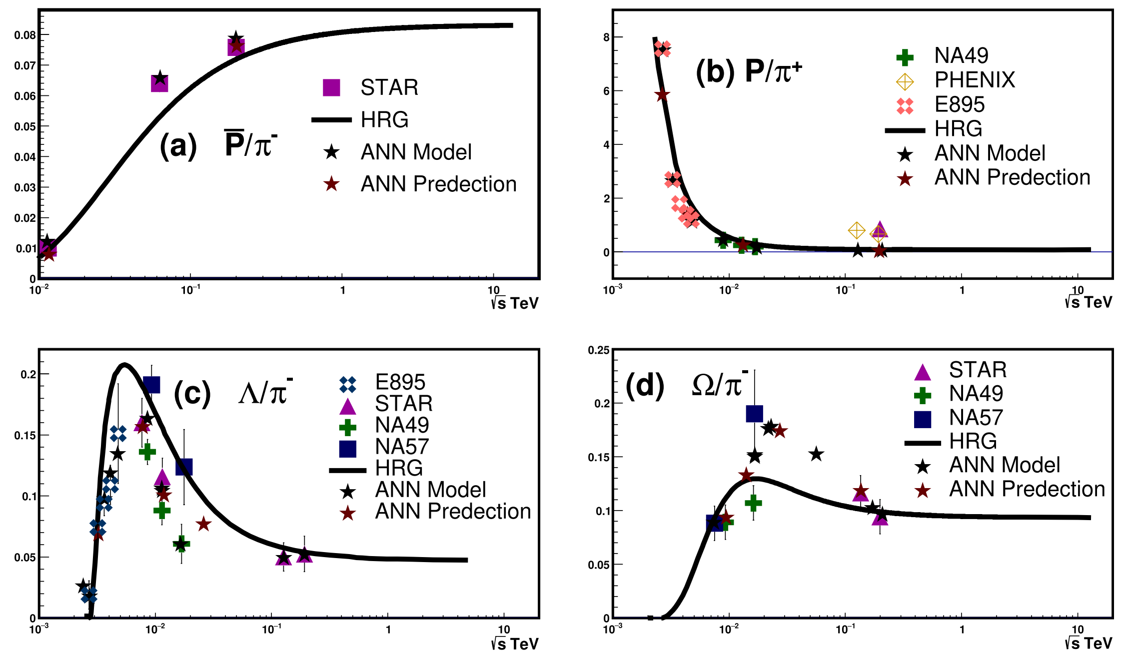

Figure 6. Model comparison for baryon-to-meson ratios: ANN model ((black asterisk)), HRG calculations (solid black lines), and experimental measurements (symbols) for: (a) $\bar{p}/\pi^-$, (b) p/π^+, (c) Λ/π^-, and (d) Ω/π^- [34–36, 38–41, 47, 57]. ANN prediction model is represented by (heavy red asterisk).

3.1.3. Baryon-to-meson ratios as a function of $\sqrt{s}$

This subsection explores the variation of baryon-to-meson particle ratios with respect to the center-of-mass energy $\sqrt{s}$, which provides essential information about baryon production mechanisms and the chemical environment during hadron freeze-out. The specific ratios investigated are:

- (a) $\bar{p}/\pi^-$,
- (b) p/π^+,
- (c) Λ/π^-,
- (d) Ω/π^-.

The ANN models were individually trained for each of these ratios using corresponding experimental datasets. The network training progress is noticed, where the reduction of MSE validates the effectiveness of the learning process. The final MSE values reached were: 2.56×10^{-6} for $\bar{p}/\pi^-$, 21.1×10^{-6} for p/π^+, 147×10^{-6} for Λ/π^-, and 9.46×10^{-6} for Ω/π^-.

To further assess the quality of learning, the MSE values present the convergence behavior of each network. The smooth decline in error across training iterations confirms that the ANN models have reached stable and optimal configurations.

The results predicted by the ANN are compared with both experimental data and HRG model calculations in figure 6. The ANN outputs (dashed curves) follow the experimental trends (symbols) with high accuracy and are in good agreement with HRG estimations (solid black lines). Notably, the ANN successfully captures the suppression behavior of the Ω/π^- ratio at lower $\sqrt{s}$ values, reflecting sensitivity to multistrange baryon production thresholds.

In summary, the ANN framework delivers strong performance in replicating baryon-to-meson particle ratios over a wide range of energies. Its predictive strength is comparable to the HRG model and is particularly promising for extrapolations into lower-energy domains that will be explored at next-generation facilities such as NICA and FAIR.

We have successfully estimated all considered particle ratios using the trained ANN model, confirming its effectiveness in capturing the underlying physics of hadron production in relativistic heavy-ion collisions. The model exhibits strong generalization performance across a broad energy spectrum, effectively learning the nonlinear relationships between particle ratios and the center-of-mass energy $\sqrt{s}$. These results highlight the ANN's potential as a complementary tool to conventional theoretical models, offering predictive flexibility in both well-explored and experimentally uncharted collision regimes like NICA and FAIR.

The predicted value of any particle ratio RR, generated by the trained ANN model, can be expressed through the following forward propagation equation:

$$R = \text{purelin}[\text{net.LW}4,\ 3 \cdot \text{logsig}(\text{net.LW}3,\ 2 \cdot \text{logsig}(\text{net.LW}2,\ 1 \cdot \text{logsig}(\text{net.IW}1,\ 1 \cdot R + \text{net.b1}) + \text{net.b2}) + \text{net.b3}) + \text{net.b4}] \quad (10)$$

In this formulation:

- RR denotes the input variable, which corresponds to the center-of-mass energy $\sqrt{s}$,
- `net.IW1,1` is the matrix of weights between the input node and the first hidden layer,
- `net.LW2,1`, `net.LW3,2`, and `net.LW4,3` are the layer-wise weight matrices that connect consecutive hidden layers and the output layer,
- `net.bi` represents the bias associated with layer ii, where i = 1,2,3,4i = 1,2,3,4,
- `logsig` is the logistic sigmoid activation function applied at all hidden layers to introduce nonlinearity,
- `purelin` is the linear activation function applied at the final output layer to yield a continuous value.

This forward-pass structure encapsulates the behavior of a fully connected, feedforward ANN with three hidden layers, enabling it to model the complex, non-linear dependence of particle ratios on collision energy. The architecture was specifically designed to learn from data and generalize well across both measured and extrapolated energy regimes in high-energy nuclear collisions.

3.1.4. Physics interpretation and outlook

With the corrected freeze-out parameters, a clearer physical interpretation of the energy dependence of the particle ratios emerges. The ratio $\bar{p}/p$ is largely governed by the baryon chemical potential $\mu_B(\sqrt{s_{NN}})$, and the HRG calculations capture the expected monotonic decrease of this ratio as the collision energy increases. This reflects the diminishing net-baryon density at mid-rapidity and is consistent with the chemical freeze-out picture established in earlier studies.

Ratios involving strange hadrons, such as K/π, Λ/π, and Ω/π, provide further insight into the role of strangeness in the hadronic medium. At low beam energies, deviations between HRG predictions and data can arise from canonical suppression of strangeness due to the small number of strange quarks in the system. As the energy increases, these effects become less pronounced and the HRG model offers a more accurate description. The present ANN analysis follows these trends and reproduces the qualitative structure seen in the data.

The ANN model, while using only $\sqrt{s_{NN}}$ as input, captures broad features of the energy dependence, but it does not encode specific physical constraints such as resonance feed-down, conserved charges, or partial strangeness saturation. Incorporating additional physics-motivated inputs such as T, μ_B, or a strangeness saturation parameter γ_s offers a promising direction for extending the present framework. Such an approach would allow the ANN to serve as a hybrid model that interpolates between first-principles expectations and data-driven learning. This may improve the diagnostic power of the model, particularly at energies relevant for NICA and FAIR, where the balance between baryon density and strangeness production is expected to be most sensitive to the underlying QCD dynamics.

These considerations provide a broader physical context for the present HRG and ANN results and offer potential avenues for integrating machine-learning approaches with established theoretical models in heavy-ion physics.

4. Conclusions

In this study, we employed artificial neural networks (ANNs) to model and predict a diverse set of particle yield ratios produced in relativistic heavy-ion collisions across a broad spectrum of center-of-mass energies. The analysis incorporated multiple categories of ratios, including antiparticle-to-particle, strange-to-non-strange meson, and baryon-to-meson combinations. These were evaluated using experimental results from AGS, SPS, RHIC, and extrapolated to future facilities such as NICA and FAIR.

To assess the reliability of the ANN-based predictions, we benchmarked them against outcomes generated using the Hadron Resonance Gas (HRG) model. While both models offered reasonable descriptions of the observed ratios, the ANN consistently demonstrated closer alignment with experimental data, particularly in the intermediate-to-low energy domain where HRG results begin to diverge.

The ANN methodology exhibited robust learning performance, achieving low mean squared error values across all ratios. Its ability to capture complex, nonlinear dependencies between particle production and collision energy highlights its advantage over more conventional equilibrium models. These results underscore the utility of ANN-based frameworks in nuclear phenomenology and support their application in interpreting upcoming experimental programs at NICA and FAIR.

Funding

The authors declare that no funding was received for this work.

Acknowledgments

The authors would like to express their sincere appreciation to Sergey Nedelko, Evgeni Kolomeitsev, and the team at the Laboratory of Theoretical Physics, JINR, for their generous hospitality and valuable support throughout the course of this work. We also acknowledge the Egyptian Academy of Scientific Research and Technology (ASRT) for funding this study within the framework of the ASRT-JINR cooperation program (Call-2023), which enabled the research activities to be conducted at the Joint Institute for Nuclear Research (JINR), Dubna, Russia.

Conflicts of interest

The authors declare no conflict of interest.

Data availability statement

All data that support the findings of this study are included within the article (and any supplementary files).

References

[1] Abramchuk R A and Selch M 2024 *Eur. Phys. J. C* **84** 107
[2] Arjun K, Vinodkumar A M and Bannur V M 2025 *Eur. Phys. J. Plus* **140** 215
[3] Cleymans J and Elliott D E A 1998 *Phys. Rev. C* **57** 3319
[4] Megias E, Arriola E R and Salcedo L L 2013 *Nucl. Phys. B Proc. Suppl.* **234** 313
[5] Bashir R, Shehzadi R, Ashraf M U and Khan A M 2025 Predictions for identified hadron ($\pi^{\pm}$, $K^{\pm}$ and $p(\bar{p})$) *Eur. Phys. J. Plus* **140** 1211
[6] Vovchenko V 2020 *Int. J. Mod. Phys. E* **29** 2040002
[7] Lao H-L, Gao Y-Q and Liu F-H 2019 *Universe* **5** 152
[8] Mohi Ud Din I, Uddin S, Parra R A, Mir S A and Rather N A 2025 *J. Subatomic Part. Cosmol.* **4** 100103
[9] Zhang X, Zhang Y, Luo X and Xu N 2025 arXiv:2506.18832
[10] Wan J, Wang C-Z, Ma Y-G, Shou Q-Y and Zhang S 2025 Particle species dependence of elliptic flow fluctuations in Pb-Pb collisions at energies available at the CERN Large Hadron Collider in a multiphase transport model *Phys. Rev. C* arXiv:2507.04497
[11] Hanafy M and Maher M 2021 *Adv. High Energy Phys.* **2021** 6660872
[12] Hanafy M and Maher M 2021 Particle Ratios within a statistically corrected hadron resonance gas model and EPOS event-generator at AGS, SPS, RHIC and LHC Energies *2109.03701* 2109.03701 2021arXiv:2109.03701
[13] Ding C, Ke W-Y, Pang L-G and Wang X-N 2021 *Chin. Phys. C* **45** 074102
[14] Niida T and Miake Y 2021 *AAPPS Bull* **31** 12
[15] Jena A K and Panda S 2025 *J. Subatomic Part. Cosmol.* **3** 100016
[16] Du L, An X and Heinz U 2021 *Phys. Rev. C* **104** 064904
[17] Duarte J and Vlimant J-R 2020 Graph Neural Networks for Particle Tracking and Reconstruction *Artificial Intelligence for High Energy Physics* 387–436
[18] Mallick N, Tripathy S, Mishra A N, Deb S and Sahoo R 2021 *Phys. Rev. D* **103** 094031
[19] Radovic A *et al* 2018 *Nature* **560** 41
[20] Pang L-G *et al* 2019 Nuclear Physics A *The 27th International Conference on Ultrarelativistic Nucleus-Nucleus Collisions: Quark Matter 2018* 982 867
[21] Pang L-G 2021 Nuclear Physics A *The 28th International Conference on Ultra-relativistic Nucleus-Nucleus Collisions: Quark Matter 2019* 1005 121972
[22] Brouwer W J, Kubicki J D, Sofo J O and Giles C L 2014 An investigation of machine learning methods applied to structure prediction in condensed matter (https://doi.org/10.48550/arXiv.1405.3564)
[23] Taranenko A 2020 *J. Phys. Conf. Ser.* **1685** 012021
[24] Tawfik A N *et al* 2016 *The European Physical Journal A* **52** 1
[25] Chen Y *et al* 2025 *Nucl. Instrum. Meth. A* **1075** 170435
[26] Habashy D M, El-Bakry M Y, Scheinast W and Hanafy M 2022 *Chin. Phys. C* **46** 073103
[27] Habashy D M, El-Bakry M Y, Tawfik A N, Abdel Rahman R M and Hanafy M 2022 *Int. J. Mod. Phys. A* **37** 2250002
[28] Tawfik A N, El-Bakry M Y, Habashy D M, Mohamed M T and Abbas E 2015 *Int. J. Mod. Phys. E* **24** 1550067
[29] Rojas R 1996 *Neural Network: A Systematic Introduction* (Springer)

[30] Stachel J and Braun-Munzinger P 1989 *Phys. Lett. B* **216** 1
[31] Haykin S 2008 *Neural Networks and Learning Machines* 3rd edition (Pearson Prentice Hall)
[32] Abd El-Rehim D A, Habashy D, Zahran H and Soliman H 2021 *Met. Mater. Int.* **2021** 2021
[33] Abd El-Rehim A F, Zahran H Y, Habashy D M and Al-Masoud H M 2020 *Crystals* **10** 2020
[34] Afanasiev S *et al* 2002 *Phys. Lett. B* **358** 275
[35] Alt C *et al* 2005 *Phys. Rev. Lett.* **94** 192301
[36] Antinori F *et al* 2004 *Phys. Lett. B* **595** 68
[37] Klay J *et al* 2003 *Phys. Rev. C* **68** 054905
[38] Chung P *et al* 2003 *Phys. Rev. Lett.* **91** 202301
[39] Pinkenburg C and E895 collaboration 2002 *Nucl. Phys. A* **698** 495–8
[40] Afanasiev S, Anticic T and Barna e a 2002 *Phys. Rev. C* **66** 054902
[41] Klay J *et al* 2002 *Phys. Rev. Lett.* **88** 102301
[42] Tawfik A N and Mishustin I 2019 *J. Phys. G: Nucl. Part. Phys.* **46** 125201
[43] Braun-Munzinger P and Stachel J 2002 *J. Phys. G28* 1971
[44] Andronic A, Braun-Munzinger P, Stachel J and Winn M 2012 *Phys. Lett. B* **718** 80
[45] Samanta S, Chatterjee S and Mohanty B 2019 *J. Phys. G: Nucl. Part. Phys.* **46** 065106
[46] Karsch F 2005 *J. Phys. G: Nucl. Part. Phys.* **31** S633
[47] Tawfik A N 2014 *Int. J. Mod. Phys. A* **29** 1430021
[48] Andronic A, Braun-Munzinger P and Stachel J 2006 *Nucl. Phys. A* **772** 167
[49] Tanabashi M *et al* 2018 *Phys. Rev. D* **98** 030001
[50] Gershenson C 2003 Artificial Neural Networks for Beginners (https://doi.org/10.48550/arXiv.cs/0308031)
[51] Kröse B, Krose B, van der Smagt P and Smagt P 1993 *J. Comput. Sci.* **48**
[52] Shanmuganathan S 2016 *Artificial Neural Network Modelling: An Introduction* **628** 1–14
[53] Hornik K, Stinchcombe M and White H 1989 *Neural Netw.* **2** 359
[54] Anil M U, Banerjee K, Malik T and Providência C 2022 *J. Cosmol. Astropart. Phys.* JCAP01(2022)045
[55] Pandey D S, Das S, Pan I, Leahy J J and Kwapinski W 2016 *Waste Manage.* **58** 202213
[56] El-Bakry M 2003 *Chaos, Solitons Fractals* **18** 995
[57] Back B *et al* 2004 *Phys. Rev. C* **69** 054901